Biosensors and Bioelectronics 24 (2008) 606–612

Contents lists available at ScienceDirect

Biosensors and Bioelectronics

journal homepage: www.elsevier.com/locate/bios

# Real-time protein biosensor arrays based on surface plasmon resonance differential phase imaging

C.L. Wong[a], H.P. Ho[a,*], Y.K. Suen[b], S.K. Kong[b], Q.L. Chen[a], W. Yuan[a], S.Y. Wu[a]

[a] Department of Electronic Engineering, The Chinese University of Hong Kong, Hong Kong, Hong Kong, China
[b] Department of Biochemistry, The Chinese University of Hong Kong, Hong Kong, Hong Kong, China

ARTICLE INFO

*Article history:*
Received 29 February 2008
Received in revised form 18 April 2008
Accepted 4 June 2008
Available online 17 June 2008

*Keywords:*
Surface plasmon resonance
Differential phase measurement
SPR phase imaging
Protein array
Microarray
Label-free

ABSTRACT

This paper reports the application of differential phase surface plasmon resonance (SPR) imaging in two-dimensional (2D) protein biosensor arrays. Our phase imaging approach offers a distinct advantage over the conventional angular SPR technique in terms of utilization efficiency of optical sensor elements in the imaging device. In the angular approach, each biosensor site in the biosensor array requires a linear array of optical detector elements to locate the SPR angular dip. The maximum biosensor density that a two-dimensional imaging device can offer is a one-dimensional SPR biosensor array. On the other hand, the phase-sensitive SPR approach captures data in the time domain instead of the spatial domain. It is possible that each pixel in the captured interferogram represents one sensor site, thus offering high-density two-dimensional biosensor arrays. In addition, our differential phase approach improves detection resolution through removing common-mode disturbances. Experimental results demonstrate a system resolution of $8.8 \times 10^{-7}$ RIU (refractive index unit). Real-time monitoring of bovine serum albumin (BSA)/anti-BSA binding interactions at various concentration levels was achieved using a biosensor array. The detection limit was 0.77 μg/ml. The reported two-dimensional SPR biosensor array offers a real-time and non-labeling detection tool for high-throughput protein array analysis. It may find promising applications in protein therapeutics, drug screening and clinical diagnostics.



## 1. Introduction

Proteomics, which refers to the analysis of proteins on a large-scale, has become one of the spotlights in today's biomedical research (Pandey and Mann, 2004; MacBeath, 2002; Phizicky et al., 2003; Melton, 2004). Defining the function of every protein in the cell is the key for solving a range of health related issues, including better understanding of disease process, early detection of disease and accelerating drug development (Hanash, 2003). While the human genome is known to contain about 40,000 genes, the human proteome is predicted to have a size of 1 million. There is certainly a great demand for developing high-throughput tools for rapid protein analysis. Conventional protein–protein interaction analysis techniques involve protein purification followed by a detection step such as sodium dodecyl-sulfate polyacrylamide gel electrophoresis (SDS-PAGE) and Western blots (Kim et al., 2006). These procedures are known to be very time consuming, and they are also not designed for high-throughput measurements.

In recent years, the protein micro-array chip has become an attractive high-throughput alternative for protein–protein interaction analysis (Kambhampati, 2004). Hundreds or thousands protein samples are spotted in a single protein micro-array and a wide variety of protein interactions and activities are analyzed simultaneously (Zhu et al., 2001). Typically, signal transduction is based on fluorescence labeling (Phizicky et al., 2003; Zhu et al., 2001). However, it is also well known that labeling tags may modify protein activities, which can lead to cross-sensitivity between sensor elements, unexpected binding or degradation in sensitivity limit.

Surface plasmon resonance imaging (SPRI) is a label-free affinity detection technique that relies on detecting the refractive index change caused by immobilization of biomolecules to the metallic sensor surface. Typically, the surface plasmon resonance (SPR) image of the entire sensing surface is captured by a charge-coupled device (CCD). SPRI biosensor provides a two-dimensional (2D) quantitative information map over the entire sensing surface, which makes it highly suitable for monitoring binding interactions in protein arrays (Homola, 2003). Until now, most SPRI biosensors are based on detecting intensity variations at a fixed angle of

* Corresponding author. Tel.: +852 2609 8279; fax: +852 2603 5558.
*E-mail addresses:* clwonglok@yahoo.com.hk (C.L. Wong), hpho@ee.cuhk.edu.hk (H.P. Ho).

0956-5663/$ – see front matter © 2008 Elsevier B.V. All rights reserved.
doi:10.1016/j.bios.2008.06.013

incidence (Yeatman and Ash, 1987; Rothenhäusler and Knoll, 1988). This approach has been shown to be useful for the detection of the binding reactions of DNA (Lee et al., 2001; Smith et al., 2002, 2003a), peptide (Wegner et al., 2002), protein–DNA (Wegner et al., 2003) and protein–carbohydrate (Smith et al., 2003b). Recently, it has also been used for protein expression analysis (Jung et al., 2004) and protein chip detection (Melton, 2004; Kim et al., 2005). The major challenge of intensity SPRI biosensors is its limited resolution (Fu et al., 2004; Homola et al., 2003). Nelson et al. (1996) proposed a high sensitivity SPR detection scheme based on phase modulation. It was estimated to have three times higher resolution than conventional SPR sensing techniques. Experimental results reported by Nikitin et al. (2000) also demonstrated sensitivity improvement using phase modulation SPRI in comparison to intensity imaging. More recently, experiments on phase SPRI were also performed by Ho and Lam (2003) and Yu et al. (2005). However, phase detection schemes reported by Ho and Lam and Yu et al. are based on analyzing interference fringes in the captured interferograms, which inevitably sacrifices spatial resolution as a large number of image pixels are used for extracting the phase of each biosensor element.

In this paper, we report a new approach for high spatial resolution phase-sensitive SPRI. Interference images are captured continuously during phase stepping in the time domain in order to enable accurate phase extraction for each pixel in the image. This also means that each pixel in the interferogram may act as an individual biosensor site, thereby providing the possibility of achieving high-density high-throughput protein arrays. Our system also makes use of a differential phase scheme (Wu et al., 2004) to eliminate common mode noise. As a demonstration of the phase-sensitive SPRI sensor, we performed experiments to monitor protein binding in a two-dimensional array of biosensors. On the gold sensor surface, we fabricated a two-dimensional array of antigen dots containing different immobilization concentrations. As an analyte containing the target antibody was introduced into the flowcell, the SPRI system monitored the antigen–antibody binding interactions at each antigen dot in real-time. Through this we have demonstrated that our two-dimensional phase SPRI technique offers a rapid, non-labeling and real-time detection tool for high-throughput protein arrays.

## 2. Experiment

### 2.1. Polydimethylsiloxane (PDMS) microwell array

A $5 \times 5$ microwell array for protein array immobilization was fabricated using PDMS. In the fabrication process, liquid form PDMS solution at room temperature was poured into a molding jig. After a baking process at 80 °C for 5 h, the PDMS became solidified and a microwell array was formed. The volume of each microwell is 5 μl. It allows 25 different protein samples to be immobilized simultaneously on the sensor surface within an area of 1.5 $cm^2$. The sensor count in the microwell array can be increased if necessary in future experiments.

### 2.2. Surface chemistry of protein array immobilization

A thin layer of gold with a nominal thickness of 50 nm was deposited on a glass prism surface by sputtering. The gold surface was immersed in ethanol containing 11-mercapto-undecanoic acid (MUA) for 17 h. This resulted in creating a self-assembled monolayer (SAM) of MUA on the gold surface. The modified surface was then rinsed by ethanol and distilled water. A mixture of *N*-hydroxy succinimide (NHS) and 1-ethyl-3-(3-dimethylaminopropyl) carbodiimide (EDC) in distilled water was prepared for surface activation. In the actual protein immobilization experiment, the NHS/EDC mixture was added to each of the antigen samples at different pre-defined ratios. The sample solutions were transferred to the microwells in the PDMS array. The microwells were emptied after 2 h of incubation time, and this resulted in the formation of an array of antigen spots on the gold sensor surface. In order to block the un-reacted regions on the sensor surface, the spots were further exposed to the ethanolamine solution for 2 min. The spots were then rinsed and stored in phosphate-buffered saline (PBS) for further protein binding reactions.

### 2.3. The optical system

A schematic of our phase-sensitive SPRI system is shown in Fig. 1. A linearly polarized He–Ne laser is used as the light source.

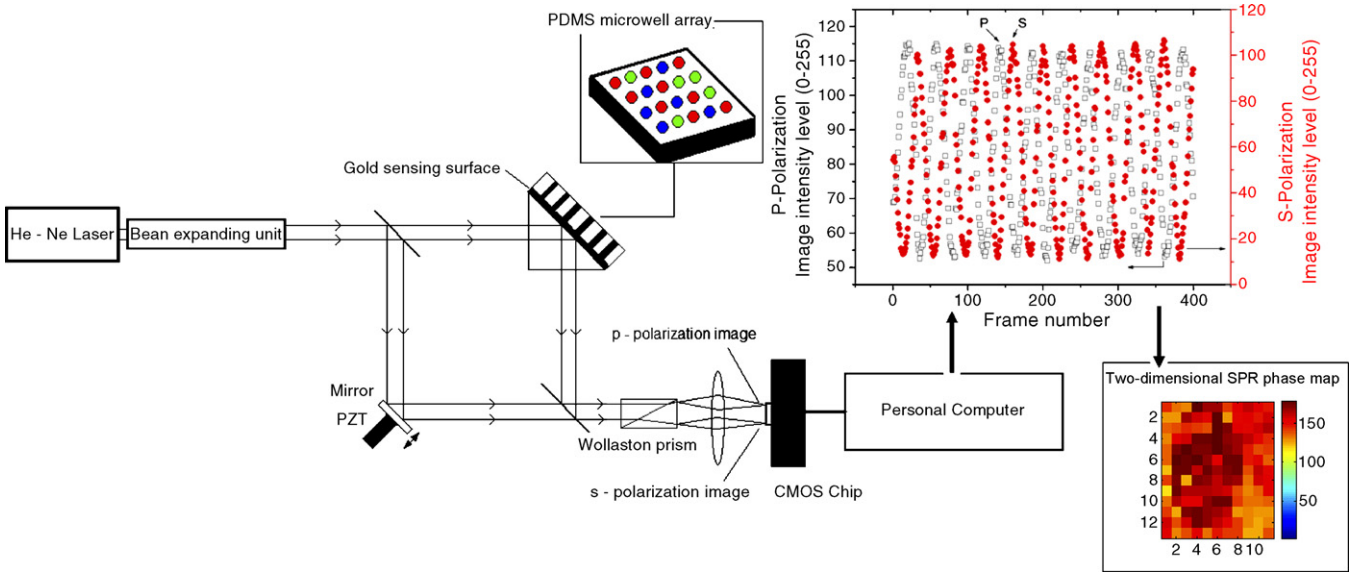


**Fig. 1.** Experimental configuration of phase SPR imaging sensor. The interference images (in video format) of p- and s-polarization were captured using a CMOS camera. Each image is divided into pixel groups (typically $50 \times 50$). For each pixel group, the interference intensity variation with respect to time (a truncated sine function) is recorded. The differential phase between p- and s-polarization is found from measuring the relative shift between the two traces, and a color map is used for displaying the phase distribution.

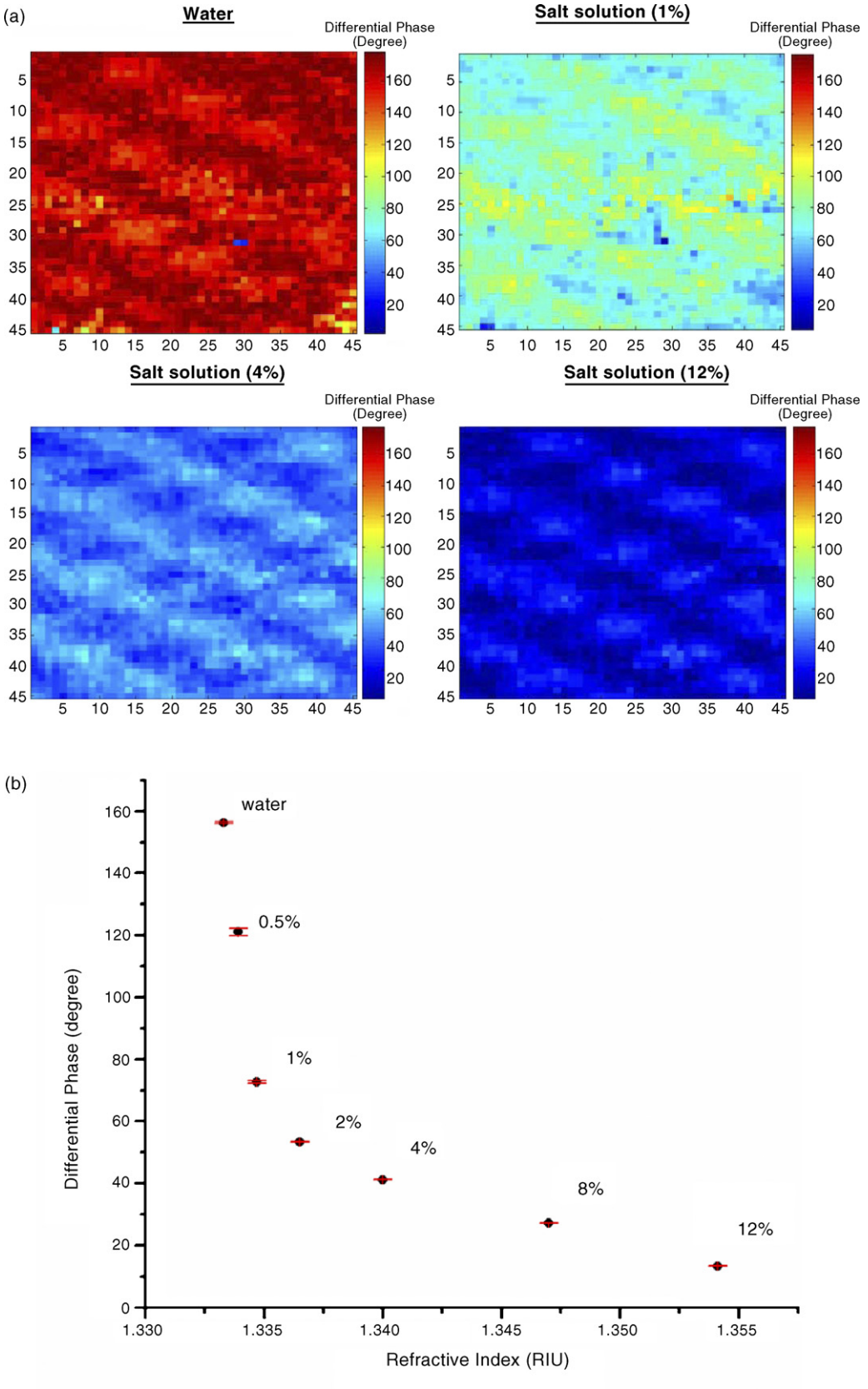


**Fig. 2.** (a) SPR phase images obtained from salt–water mixtures: pure water (0%), 1, 4 and 12% (averaged phase image among 35 video clips). (b) The plot of differential phase shift vs. refractive index. (Measurement on each sample has been repeated for 32 times to improve measurement resolution. The error bars are the S.D. of the averaged data points, which is obtained by taking the average of every 4 measurements, as it has been found that averaging involving more than 4 measurements does not provide any further improvement on the S.D.)

A beam expander set converts the laser beam to about 30 mm in diameter. We use a Mach–Zehnder (M–Z) interferometer for phase detection. In the probe arm ($I_{probe}$), the beam is reflected by the sensor surface by an inverted prism arrangement (also called the Kretschmann configuration). In the reference arm ($I_{ref}$), the mirror mounted on a piezoelectric transducer (PZT) serves as a beam-folding device as well as an optical phase shifter. The PZT is driven by a saw-tooth wave signal typically at 0.03 Hz. The maximum linear phase shift in the reference arm is approximately $12\pi$. After passing through a Wollaston prism, two optical beams coming from the p- and s-polarization are obtained. The interference images from these two orthogonal polarizations are projected on the two halves within the same CMOS imaging chip. Interference images due to p- and s-polarization are divided into a matrix of pixel groups (typically $50 \times 50$). In the present case, the size of each pixel is 150 μm. With the PZT continuously shifting the reference optical phase, intensity variations captured at pixel level in the output arm of the M–Z interferometer will follow a truncated sine function. The frame sequence recorded by the imaging device actually represents the raw data of our SPRI technique. Fast Fourier transform (FFT) combined with appropriate signal processing will convert the raw data into a two-dimensional SPR phase map that has direct correlation with the protein binding activity taking place at each sensor site. As s-polarization light is not affected by SPR excitation, the SPR phase map due to s-polarization can serve as a reference. Pixel-wise phase subtraction between the data obtained from s- and p-polarization will provide the final SPR phase map. This differential SPR phase measurement approach is an effective way to eliminate common path noise caused by mechanical drift (Fig. 1).

## 3. Results and discussion

To estimate the performance of our SPRI system, we performed experiments to measure the shift in refractive index caused by dissolving salt in water. Salt–water mixtures with solute concentration between 0 and 12% in weight ratio were used as the samples. The corresponding refractive index range was between 1.3330 and 1.3541 RIU. In the experiment, an incident angle near the SPR angular dip of water was chosen. Fig. 2a shows the phase maps for 0%, 1%, 4% and 12% salt concentrations. As the concentration increases from 0 to 1%, 4 and 12%, the color (differential phase response) of the SPR phase map changes from red to yellow-blue, light-blue and dark-blue, respectively. For each phase map, we also calculated the mean differential phase value of the entire SPR phase map. Fig. 2b shows a plot between the mean differential phase and salt concentration. In the most sensitive region of the response curve, we found a phase change of 83.5° for the refractive index range of 1.3330–1.3347 RIU (Fig. 2).

We also estimated the measurement fluctuation of the system by monitoring the standard deviation (S.D.) of the phase data collected from a sample containing 8% of salt. The monitoring period was 20 min. Fig. 3 reveals that the measurement S.D. decreases with increasing number of data points used for averaging, but no further improvement is observed when more than four data points are used. This is believed to be related to measurement drifts caused by environmental fluctuations, e.g. temperature variations, which cannot be removed by data averaging. If we take the mean S.D. of 0.043° as the minimum phase measurement that the system can resolve, the estimated sensor resolution is $8.8 \times 10^{-7}$ RIU.

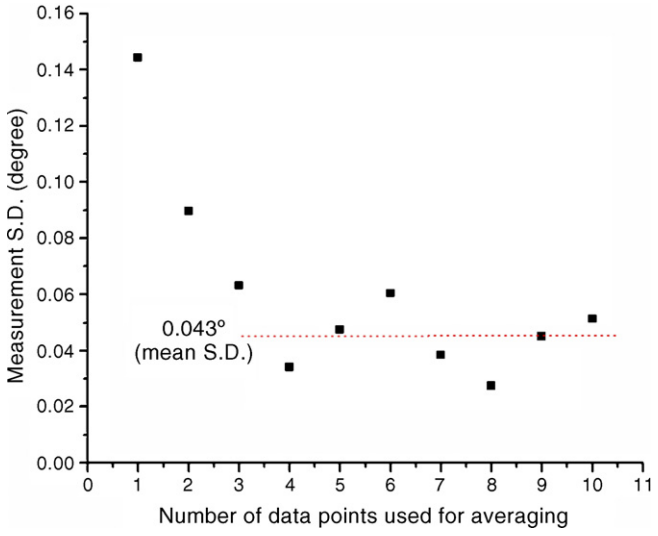


**Fig. 3.** S.D. of phase measurement obtained from 8% salt–water mixture. The plot shows the expected trend of decreasing S.D. as the number of measurements increases. When the number of data point used for averaging is higher than 4, no significant reduction in S.D. has been observed. The "saturated" S.D. of 0.043° is obtained by calculating the mean of all data point from 4 to 10.

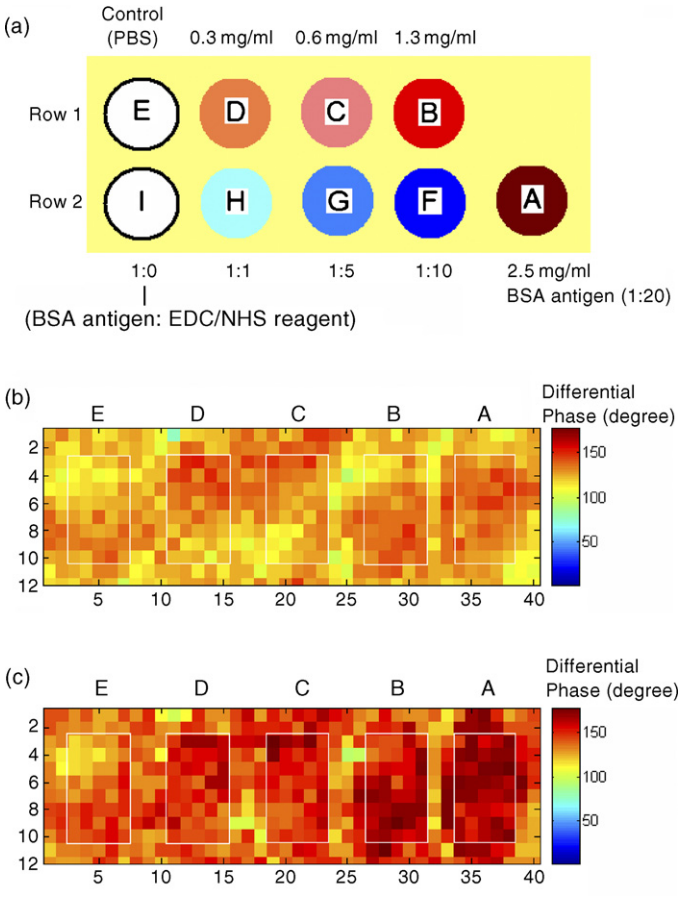


**Fig. 4.** (a) Schematic of the protein array. In protein spots (A–D), the sensor sites were incubated with NHS/EDC surface activation reagent in the ratio of 1:20. The bovine serum albumin (BSA) antigen concentrations used in the sensor sites were 2.5 mg/ml (A), 1.3 mg/ml (B), 0.6 mg/ml (C) and 0.3 mg/ml (D). PBS was incubated in spot E as a control for observing the non-specific binding during the experiment. In protein spots A, F, G, H and I, the incubation ratios between BSA and NHS/EDC mixture were varied in order to find the optimized incubation ratio between BSA antigen and EDC/NHS surface activation reagent. The ratios were varied from 1:20, 1:10, 1:5, 1:1 to 1:0 in spot A, F, G, H, I, respectively. (b) The SPR phase image taken when exposing the protein array to PBS buffer. (Averaged between 0 and 33 min) (c) Final (equilibrium) SPR phase image taken when no further antigen–antibody binding activity was observed. (Averaged between 71 and 89 min)

In fact, the system S.D. can also be estimated by finding the mean of the S.D. obtained from different salt–water samples. From our experiments, the mean of the S.D. is 0.36°. If we use this value as the system uncertainly, the corresponding sensor resolution is $7.3 \times 10^{-6}$ RIU. The reason for such a higher value in comparison to the one calculated in the previous case is that the measurement uncertainty increases for low concentration solutions (water, 0.5%, 1%) (as indicated in the error bar of the response curve). It is because that the contrast of the p-polarization interference pattern is greatly reduced when the incident angle is near the SPR dip. In future experiment, an intensity attenuator can be used to reduce the optical power of the reference beam in order to enhance the contrast of the p-polarization inference image (Fig. 3).

### 3.1. Protein binding experiments

In order to evaluate the potential of phase-sensitive SPRI for arrayed protein binding detection, experiments were conducted to monitor specific binding reaction between bovine serum albumin (BSA) antigen and antibody. The PDMS microwells were loaded with BSA antigen–PBS samples containing different concentrations of BSA antigen (Fig. 4a). For spots labeled A to D, the BSA antigen samples were incubated with (NHS)/(EDC) surface activation reagent in the ratio of 1:20 for 2 h. The BSA antigen concentrations for spots A–D are 2.5, 1.3, 0.6 and 0.3 mg/ml, respectively. Only PBS buffer was incubated in spot E as a control for monitoring any non-specific binding that might take place during the experiment.

First, the protein array was exposed to PBS buffer and the corresponding SPR phase image is shown in Fig. 4b. After that, anti-BSA antibody (0.025 mg/ml) was added to the protein array and the subsequent antigen–antibody binding reactions taking place at the sensor sites were recorded using the SPRI system. Fig. 4c shows an equilibrium phase map taken when all the binding reactions had saturated. Comparison between these 2 phase maps reveals that the color of the high concentration spots (A and B) has changed from orange to dark red, while the low concentration spots (C and D) exhibit a color change from orange to red. Our results therefore qualitatively confirm the expectation that higher concentration of protein binding should result in larger SPR phase change. In the phase images of the control spot (E), the phase response changed from light orange to dark orange after the exposure to the anti-BSA antibody. The phase change indicates the amount of non-specific binding occurring during the binding interaction and the non-specific binding is believed to be mainly caused by the physical attachment of BSA antibody on the sensor surface. Furthermore, relatively low phase response was recorded in the control spot (E) comparing to that recorded in spots A–D. It proves that the binding interactions in spot A–D are due to specific binding interactions between BSA antigen and anti-BSA antibody (Fig. 4).

For more quantitative measurement of the SPR phase, a procedure to calculate the average of all the pixel groups in each spot (i.e. inside the white squares in Fig. 4b and c) was performed. To further improve phase measurement resolution, the average SPR phase values obtained from five phase maps are averaged to find SPR phase value for the spot. Quantitative SPR phase response curves for the spots containing different concentrations of BSA antigen are shown in Fig. 5. The curves indicate that both the binding rate and the equilibrium phase change in the spots containing high BSA–antigen concentrations, i.e. 2.5 mg/ml (A) and 1.3 mg/ml (B), are higher than those from low concentrations, i.e. 0.6 mg/ml (C), 0.3 mg/ml (D) and the control (E). Fig. 6 further confirms that the equilibrium SPR phase change for 2.5 mg/ml (A) is 1.7 and 2.7 times higher than those from 0.3 mg/ml (D) and the control (E), respectively. Relatively low response is recorded in the control (E). This means that non-specific binding is not significant in experiment and the phase shifts observed in other spots (A–D) are caused by specific antigen–antibody binding interactions. We have measured the phase fluctuation within 33 min in the spot containing 1.3 mg/ml antigen (B) and the S.D. was found to be 0.88°. The injection of 0.025 mg/ml anti-BSA in spot B resulted in a SPR

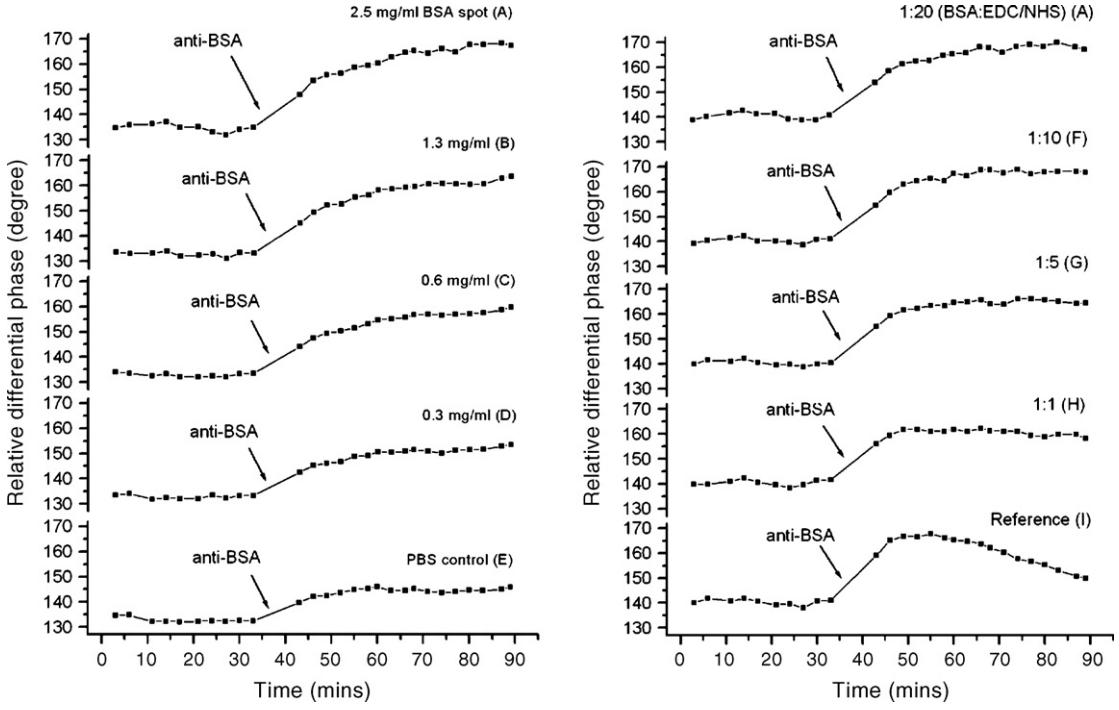


**Fig. 5.** Quantitative analysis of the antigen–antibody interaction in each protein spot. The phase shifts from the pixel groups in the SPR phase map (inside the white squares in Fig. 4b and c) are averaged into one phase value. The phase value is plotted against time.

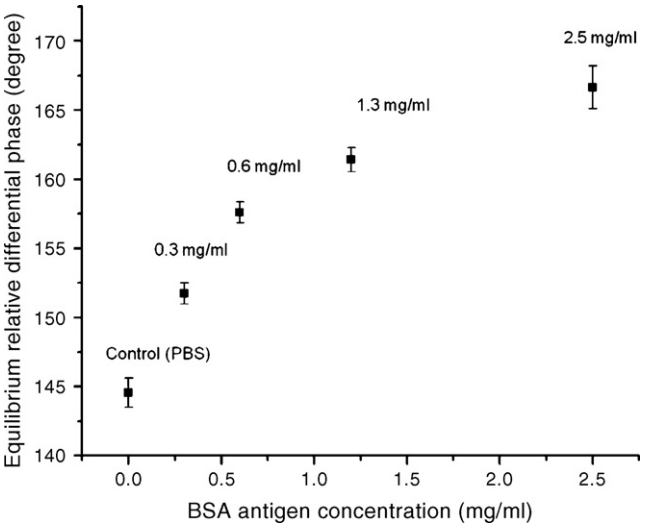


**Fig. 6.** The plot between antigen concentration and equilibrium phase shift.

phase response of 28.6°. The corresponding detection limit is calculated to be $7.7 \times 10^{-4}$ mg/ml. This value is comparable with the detection limit ($10^{-4}$ mg/ml) reported by Lee et al. (2007) for IgG antigen–antibody interaction detection.

Here, we also report a comparison on the hardware of the aforementioned system (Lee et al., 2007), in which the authors reported a similar phase-sensitive SPR imaging system incorporating a microfluidic platform. First, their design is based on a single beam phase-stepping interferometer (PSI) (Su et al., 2005) in which a liquid crystal modulator (LCM) is employed to perform 5-step phase stepping between the p- and s-polarization components. Although no clear information was presented to explain how the authors extracted the final SPR phase for each pixel, it seems that they performed a straightforward phase difference calculation using a specific region within the image as the reference. On the other hand, the present system extracts the actual SPR phase map by comparing the two data points from the reference and signal interference images for each pixel, hence making it a 100% common-path system. Moreover, the accuracy of the phase measurement depends heavily on the repeatability of the five interference images obtained upon shifting of the retardation within a $2\pi$ circle. This means that any small temperature drift in the LCM may introduce variation in the size (supposedly fixed at $\pi/4$) of the phase steps. On the other hand, in the present case, we use a moving mirror technique to perform phase sifting in small steps. This means that the system collects as much information as possible before reconstructing the sinusoidal waveforms for calculating the differential phase between the reference and signal images. Through this approach one can further improve the quality of the phase information extracted from the images.

In addition to the above, the optimization of incubation ratio between antigen and EDC/NHS surface activation reagent was explored. Antigen samples were incubated with NHS/EDC mixture in different ratios. The ratios were varied at 1:20, 1:10, 1:5, 1:1 and 1:0 in A, F, G, H and I protein spots, respectively. Spot I served as a control for monitoring any binding interaction in the absence of EDC/NHS surface treatment. The protein array was exposed to PBS buffer first. Then, anti-BSA antibody (0.025 mg/ml) was loaded to the microwells and the phase responses for different spots were recorded. Experimental phase changes are plotted against time in Fig. 5. It shows that the binding interactions observed in spot A, F, G, H are similar, while a significant drop is observed in the control spot (I). This phase drop indicates that a significant amount of antibody has dissociated from the antigen surface. This shows that the antigen–antibody binding interaction cannot take place without any surface activation by the EDC/NHS reagent. Similar binding interactions observed in spot A, F, G and H also indicates the possibility of protein immobilization using lower ratio of EDC/NHS reagent.

From the above results, a two-dimensional phase-sensitive SPRI sensor has been successfully demonstrated. This can be an effective tool for parallel monitoring of protein binding reactions in an array format. This technique may find wide applications in protein therapeutics, drug screening and clinical diagnostics (Figs. 5 and 6).

## 4. Conclusion

A two-dimensional SPR biosensor array based on time-modulated differential phase detection has been successfully demonstrated. Experimental results demonstrate that the best resolution of the system is $8.8 \times 10^{-7}$ RIU. Our experiments using BSA antigen also confirms its capability for performing real-time monitoring of protein binding reactions. A detection limit of $7.7 \times 10^{-4}$ mg/ml has been demonstrated. Our two-dimensional phase-sensitive SPR biosensor array offers a rapid, non-labeling and real-time detection tool for high throughput protein array analysis. It may find promising applications in protein therapeutics, drug screening and clinical diagnostics.

## Acknowledgements

The authors wish to acknowledge the funding support from the Research Grants Council, HKSAR, through a RGC Earmark Grant (Project # 411907) and The Shun Hing Institute of Advanced Engineering, The Chinese University of Hong Kong.

The authors would also like to acknowledge Mr. Chun Lok Wong for his assistance in recent bio-sensing experiments. His effort in data recording certainly has produced contributions to our SPR imaging project. Finally, the authors would like to thank Vanessa, Ho and Rebecca, Chow for their prayers.

## References

Fu, E., Chinowsky, T.M., Foley, J., Weinstein, J., Yager, P., 2004. Rev. Sci. Instrum. 75, 2300–2304.
Hanash, S., 2003. Nature 422, 226–232.
Ho, H.P., Lam, W.W., 2003. Sens. Actuators B: Chem. 96 (3), 554–559.
Homola, J., 2003. Anal. Bioanal. Chem. 377, 528–539.
Homola, J., Vaisocherová, H., Dostálek, J., Piliarik, M., 2003. Methods 37 (1), 26–36.
Jung, J.M., Shin, Y.B., Kim, M.G., Ro, H.S., Jung, H.T., Chung, B.H., 2004. Anal. Biochem. 330 (2), 251–256.
Kambhampati, D., 2004. Protein Microarray Technology. Wiley-VCH.
Kim, M., Jung, S.O., Park, K., Jeong, E.J., Joung, H.A., Kim, T.H., Seol, D.W., Chung, B.H., 2005. Biochem. Biophys. Res. Commun. 338 (4), 1834–1838.
Kim, M., Park, K., Jeong, E.J., Shin, Y.B., Chung, B.H., 2006. Anal. Biochem. 351 (2), 298–304.
Lee, H.J., Goodrich, T.T., Corn, R.M., 2001. Anal. Chem. 73, 5525–5531.
Lee, K.H., Su, Y.D., Chen, S.J., Tseng, F.G., Lee, G.B., 2007. Biosens. Bioelectron. 23 (4), 466–472.
MacBeath, G., 2002. Nat. Gen. 32, 526–532.
Melton, L., 2004. Nature 429, 101–107.
Nelson, S.G., Johnston, K.S., Yee, S.S., 1996. Sens. Actuators B: Chem. 35 (1–3), 187–191.
Nikitin, P.I., Grigorenko, A.N., Beloglazov, A.A., Valeiko, M.V., Savchuk, A.I., Savchuk, O.A., Steiner, G., Kuhne, C., Huebner, A., Salzer, R., 2000. Sens. Actuators A: Phys. 85 (1–3), 189–193.
Pandey, A., Mann, M., 2004. Nature 405, 837–846.
Phizicky, E., Bastiaens, P.I.H., Zhu, H., Snyder, M., Fields, S., 2003. Nature 422, 208–215.
Rothenhäusler, B., Knoll, W., 1988. Nature 332, 615–617.
Smith, E.A., Kyo, M., Kumasawa, H., Nakatani, K., Saito, I., Corn, R.M., 2002. J. Am. Chem. Soc. 124, 6810–6811.
Smith, E.A., Erickson, M.G., Ulijasz, A.T., Weisblum, B., Corn, R.M., 2003a. Langmuir 19, 1486–1492.
Smith, E.A., Thomas, W.D., Kiessling, L.L., Corn, R.M., 2003b. J. Am. Chem. Soc. 125, 6140–6148.

Su, Y.D., Chen, S.J., Yeh, T.L., 2005. Opt. Lett. 30, 1488–1490.
Wegner, G.J., Lee, H.J., Corn, R.M., 2002. Anal. Chem. 74, 5161–5168.
Wegner, G.J., Lee, H.J., Marriott, G., Corn, R.M., 2003. Anal. Chem. 75, 4740–4746.
Wu, S.Y., Ho, H.P., Law, W.C., Lin, C., Kong, S.K., 2004. Opt. Lett. 29, 2378–2381.
Yeatman, E., Ash, E., 1987. Electron. Lett. 23, 1091–1092.
Yu, X., Wang, D.X., Wei, X., Ding, X., Liao, W., Zhao, X., 2005. Sens. Actuators B: Chem. 108 (1–2), 765–771.
Zhu, H., Bilgin, M., Bangham, R., Hall, D., Casamayor, A., Bertone, P., Lan, N., Jansen, R., Bidlingmaier, S., Houfek, T., Mitchell, T., Miller, P., Dean, R.A., Gerstein, M., Snyder, M., 2001. Science 293, 2101–2105.